RSC Advances

PAPER

View Article Online
View Journal | View Issue

Cite this: *RSC Adv.*, 2019, **9**, 31440

Simultaneous detection of acetaminophen and 4-aminophenol with an electrochemical sensor based on silver–palladium bimetal nanoparticles and reduced graphene oxide

Nannan Dou, Siyu Zhang and Jianying Qu *

Received 2nd August 2019
Accepted 27th September 2019

DOI: 10.1039/c9ra05987c

rsc.li/rsc-advances

In this paper, Ag–Pd bimetallic nanoparticles uniformly distributed on reduced graphene oxide (rGO) were synthesized by redox reaction between Pd^{2+}, $Ag^{+}$and GO, and were characterized by X-ray diffractometry, field emission scanning electron microscopy, electrochemical impedance spectroscopy and thermal gravimetric analyses. A novel electrochemical sensor was constructed based on these nanocomposites using glassy carbon as a substrate. Under optimal conditions, the linear ranges were 0.50–300.00 μM for PA and 1.00–300.00 μM for 4-AP, with the detection limits of 0.23 μM for PA and 0.013 μM for 4-AP, respectively. This sensor was successfully applied to the determination of PA in pharmaceutical formulations and gave satisfactory results with a lower detection limit, wider linear range and good reproducibility.

1. Introduction

Paracetamol (PA, acetaminophen or *N*-acetyl-*p*-aminophenol) is an effective antipyretic analgesic, which is mainly used to reduce fever and relieve pain caused by headaches, surgery, and the like.[1,2] Plenty of PA prescriptions, including tablets, syrups, and so on, have been reliable and effective for all kinds of patients covering kids, the elderly, and expectant mothers.[3] However, excessive use of paracetamol may cause serious complications such as hepatotoxicity, nephrotoxicity, and pancreatic diseases.[4,5] As a reaction intermediate or decomposition product of acetaminophen, *p*-aminophenol (4-AP) has an excessive accumulation of nephrotoxicity and hepatotoxicity.[6] Therefore, the pharmacopoeia in Europe, the United States, the United Kingdom, Germany and China have set the maximum permissible limit of 4-AP in PA drug preparations at 50 ppm (0.005% w/w).[7] Thus it is very necessary to find fast, simple, reliable and accurate analytical methods to detect 4-AP and PA. Because of their unique advantages, more and more research studies have been performed on electrochemical sensors to detect 4-AP and PA.[8,9]

Graphene oxide (GO) has attracted widespread attention due to its extraordinary electron transport ability, excellent electrical conductivity, large specific surface area, strong mechanical strength and good biocompatibility.[10–12] However, GO suffers from lower electrocatalytic capabilities due to the inert nature of carbon atoms and the lack of specific active sites.[13] Therefore, in order to improve the electrical conductivity, graphene oxide needs to be reduced to reduced graphene oxide (rGO),[14] which has been used in the manufacture of electrochemical sensors.[15–17] Especially, graphene-based nanocomposites have been widely used for their unique properties.[18,19]

Precious metals having an oversized size is of great interest due to its large surface area and a large number of corner atoms and edge, which greatly enhance their catalytic activities and reduce the use of the catalyst.[20] Among the noble metals, palladium catalysts are favored by researchers because of their high catalytic activity and selectivity.[2,17] Nevertheless, commercial palladium-based catalysts are expensive and susceptible to poisoning.[21] In addition, they are impressible to air and water, and need to add an organic ligand, such as triphenyl phosphine, which not only the environment is polluted, but also causes product separation problems.[22] Heterogeneous catalysts are able to solve this problem.[23] Silver plays a supporting role in catalysis.[13,24,25] As a consequence, bimetallic nanoparticles are expected to cut the cost of catalysts and increase the resistance of the catalyst and facilitate the transfer of electrons between PA, 4-AP and the electrode surface. Chitosan (CS), which as an important natural biopolymer, can form electrochemical sensors by forming a thin film on the glassy carbon electrode and preventing Ag–Pd@rGO from falling off due to its good adhesion and film forming ability.[26–28]

In this paper, Ag–Pd@rGO nanocomposites were prepared through distributing Ag–Pd bimetallic nanoparticles uniformly on rGO, and was combined with CS prepare a novel electrochemical sensor, which have good electrocatalytic activities for PA and 4-AP. Based on this, an new method for simultaneously determination

Institute of Environmental and Analytical Sciences, College of Chemistry and Chemical Engineering, Henan University, Kaifeng, Henan 475004, P. R. China. E-mail: QJY405407@163.com; qujy@henu.edu.cn; Tel: +86-0371-22199505

of PA and 4-AP was constructed. The sensor has lower detection limit and wider linear range with better reproducibility.

2. Experimental

2.1 Reagents and apparatus

Graphene Oxide (GO), silver nitrate, palladium chloride, 4-AP and PA were all purchased from Aladdin reagent Co. Ltd (Shanghai, China). Chitosan (CS) was obtained from Huashuo Fine Chemicals Co. Ltd (Shanghai China). By mixing the stock solution of 0.1 M NaH_2PO_4 and 0.1 M Na_2HPO_4 to formulate phosphate buffer solution (PBS, 0.1 M). All the chemicals were analytical grade.

The entire experiment used the CHI650E (CHI company, USA) electrochemical workstation, with a three-electrode system, including a glassy carbon electrode (GCE) (3 mm diameter) or chemical modified glassy carbon electrodes were used as the working electrode, a platinum wire electrode as the counter electrode, and an Ag/AgCl (saturated KCl) as the reference electrode, respectively. DZF-6050 vacuum drying oven (Yi heng, China), PHS-3E pH meter (Leici, China), and DF-101S water bath pot (Great Wall, China) were also used. X-ray diffraction (XRD) patterns were performed on an X-ray D8 Advance (Bruker, Germany). An IM6ex electrochemical impedance spectroscopy analysis instrument (Zahner, Germany). The materials were also characterized by scanning electron microscope (SEM) and Energy Dispersive Spectrometer (EDS) (JSM-7610, Japan). Thermal gravimetric analyses (TGA) using a thermal analysis instrument (TGA/DSC3+, TA Instruments) from 25 °C to 500 °C under N_2 atmosphere with a heating rate of 10°C min^{-1}.

2.2 Synthesis of Ag–Pd@rGO, Pd/rGO, Ag/rGO and rGO

Ag–Pd@rGO nanocomposites were synthesized as previous report.[22] First, in a beaker, added 10 mL of GO suspension (0.5 g L^{-1}), 5 mL of $AgNO_3$ (1.23 mM) and 5 mL of $PdCl_2$ (2.46 mM). Next, the pH was adjusted to 8–9 by the addition of a dilute sodium hydroxide solution. Then, the mixed solution was heated for 1 h at 80 °C with vigorous stirring. After the solution was centrifuged and washed several times with double distilled water. The nanocomposites was dried at 60 °C in a vacuum oven to give the Ag–Pd@rGO.

The Pd/rGO was synthesized with the same method without adding $AgNO_3$. The Ag/rGO was synthesized with the same method without adding $PdCl_2$. The synthesis of rGO refers to the previous work of this group.[17]

2.3 Preparation of CS/Ag–Pd@rGO/GCE

After being burnished successively by 1.0 μm, 0.3 μm, 0.05 μm Al_2O_3 and washed with absolute ethyl alcohol and double distilled water, respectively. The surface of bare GCE was coated with 6 μL of Ag–Pd@rGO suspension (1 mg mL^{-1}) and dried to give a modified electrode (Ag–Pd@rGO/GCE). After that, 2 μL of 1% chitosan solution (2% acetic acid) was dropped onto the Ag–Pd@rGO/GCE and dried. The proposed sensor was constructed and marked as CS/Ag–Pd@rGO/GCE. Scheme 1 shows the preparation process of the electrochemical sensor.

2.4 Electrochemical method

Experiments were carried out using the cyclic voltammetry (CV) and different pulse voltammetry (DPV) methods. CV test conditions: voltage range is 0.6 V–0.2 V, scan rate is 100 mV s^{-1}. DPV test conditions: pulse width: 0.05 s; quiet time: 2 s; sampling width: 0.0167 s; voltage range: 0.6–0.2 V.

3 Results and discussions

3.1 Characterization of Ag–Pd@rGO

The morphology of rGO, Pd/rGO and Ag–Pd@rGO was characterized by SEM, shown as Fig. 1. From the Fig. 1a, the sheet

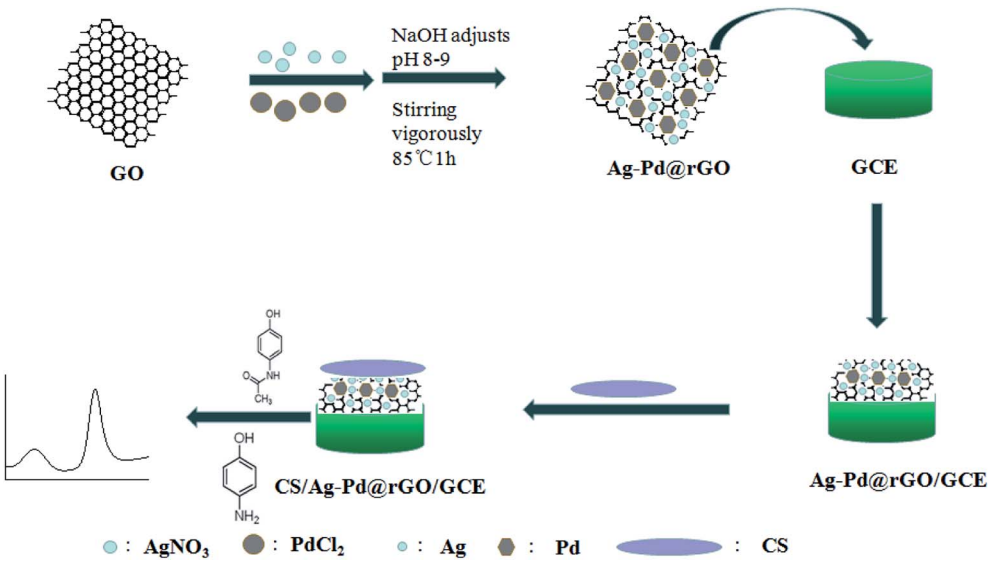

Scheme 1 Illustration of the fabrication process of the electrochemical sensor.

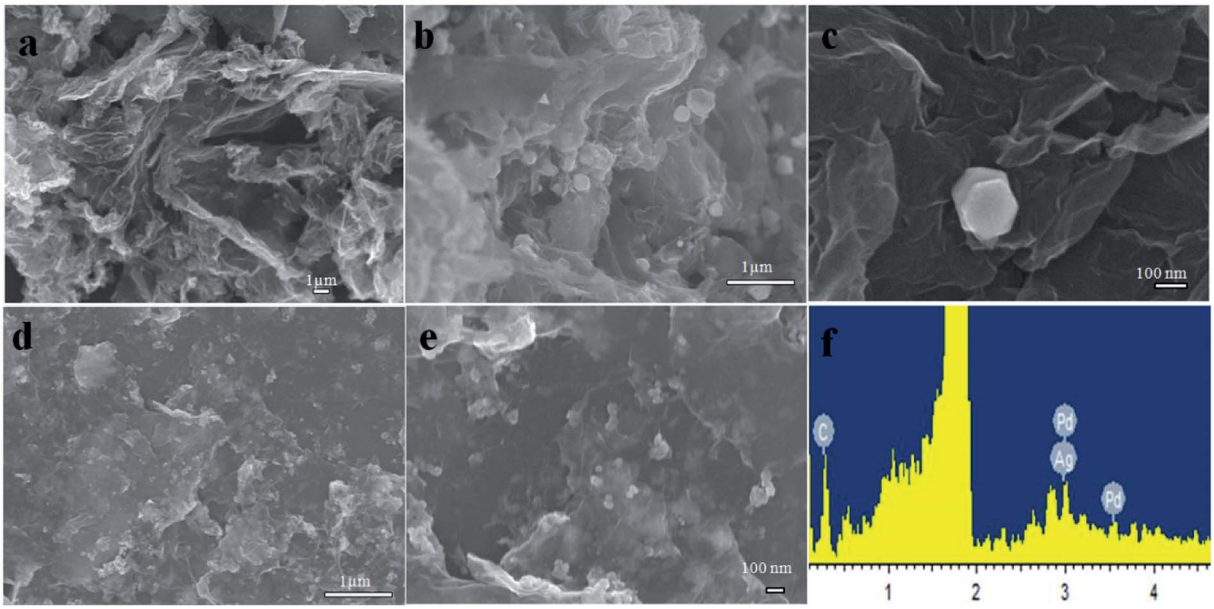

Fig. 1 SEM images of the rGO (a), Pd/rGO (b and c) and Ag–Pd@rGO (d and e) and EDS spectra of the Ag–Pd@rGO (f).

structure of rGO can be clearly seen. And from the Fig. 1c of Pd/rGO image, it can be seen that the Pd nanoparticles are hexagonal modified on the sheet structure of rGO. Fig. 1d and e is an SEM image of the Ag–Pd@rGO composite material, which can be seen clearly that the metal particles of hexagonal Pd and spherical Ag are evenly distributed on the surface of the sheet structure. Particularly, the energy spectrum analysis of Fig. 1f also confirms the presence of C, Ag and Pd in the composites. The above results indicated the successful synthesis of Ag–Pd@rGO composites.

The reduction of GO was also proved by thermal gravimetric analyses (TGA). The results are shown in Fig. 2. It can be seen that GO has two main weight losses: rapid weight loss from 30 to 150 °C (~25%) is owing to dehydration of GO, the second weight loss (~25%) at 150 to 250 °C is because of decomposition of the oxygen-containing functional groups.[29] For Ag–Pd@rGO, the second weight loss was significantly lower than that of GO, indicating that most of the oxygen-containing functional groups were removed during the reaction. This result proves that GO was reduced successfully.

Fig. 3 is an X-ray diffraction pattern of Ag–Pd@rGO. The main peak corresponds to the diffractive surface of rGO, and the diffraction peaks appearing at 35.8°, 45.6°, 62.4°, 76.4° and 82.2° correspond to (004), (103), (110), (201), and (203) diffraction of Ag. The diffraction peaks appearing at 40.1°, 46.8°, 68.4°, 82.0° and 86.7°, correspond to the (111), (200), (220), (311), and (222) diffractive planes of Pd. This result indicates the Ag–Pd@rGO composite was synthesized successfully.

Fig. 4 shows electrochemical impedance spectra of Ag–Pd@rGO/GCE (d), Pd/rGO/GCE (c), rGO/GCE (b) and GCE (a). As

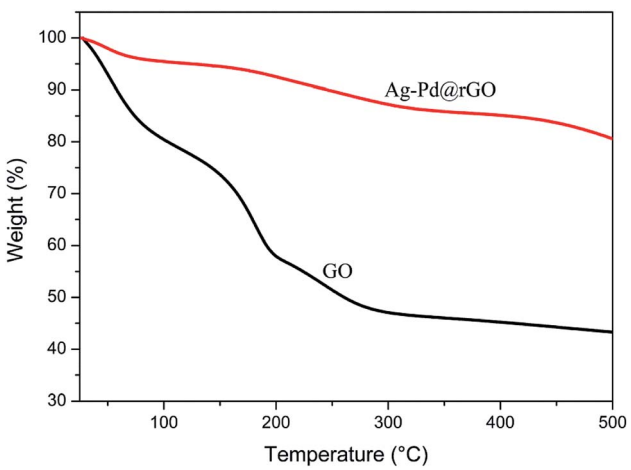

Fig. 2 TGA patterns of GO and Ag–Pd@rGO.

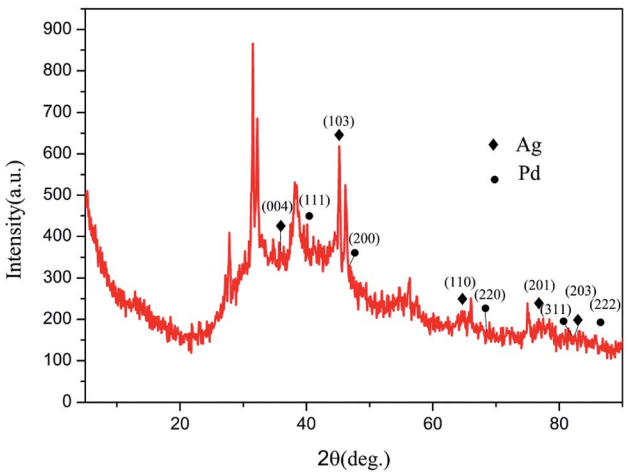

Fig. 3 The XRD spectra of the Ag–Pd@rGO.

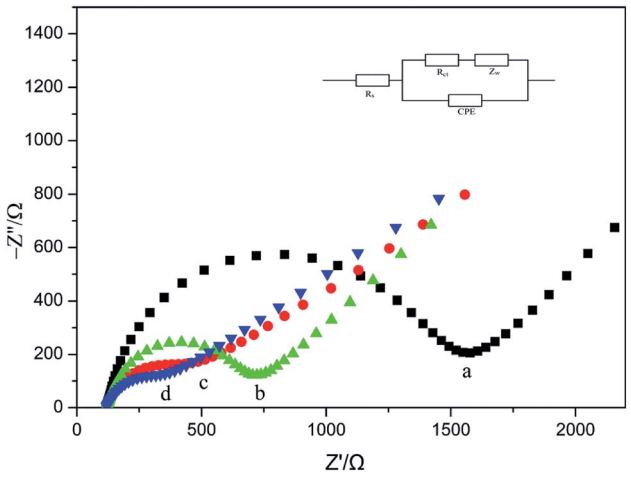

Fig. 4 Nyquist plots obtained with various glassy carbon electrodes (GCEs): GCE (a), rGO/GCE (b), rGO/Pd/GCE (c) and Ag–Pd@rGO (d) in 5.0 mM $[Fe(CN)_6]^{3-}/[Fe(CN)_6]^{4-}$.

can be seen from the figure, the unmodified GCE has an impedance of 1600 Ω, and the rGO is modified to the glassy carbon electrode, and the resistance value is remarkably lowered, it is because that the graphene has good conductivity. Furtherly, the impedance of Pd/rGO/GCE is further lowered following with modification of Pd nanoparticles. Since silver has good electrical conductivity, the impedance of Ag–Pd@rGO/GCE is further reduced compared to the impedance of Pd/rGO/GCE. All the results proved that rGO, Pd/rGO and Ag–Pd@rGO have been immobilized onto the GCE, and Ag–Pd@rGO possesses optimal electrical conductivity compared with other materials.

3.2 Electrochemical behaviors of PA and 4-AP at different electrodes

The electrochemical responding of 4-AP and PA at the GCE (f), CS/GCE (e), CS/Ag/rGO/GCE (d), CS/rGO/GCE (c), CS/Pd/rGO/GCE (b) and CS/Ag–Pd@rGO/GCE (a) in 0.1 M PBS (pH = 8) were researched by DPV, as shown in Fig. 5. From the figure, it can be observed obviously that the oxidation peaks of PA and 4-AP at 110 mV and 440 mV, respectively. And compared with the bare GCE, CS/Pd/rGO/GCE, CS/rGO/GCE and CS/Ag/rGO/GCE, CS/Ag–Pd@rGO/GCE has both highest response current and best selectivity to PA and 4-AP, which indicates that the CS/Ag–Pd@rGO composite possess excellent electrocatalytic ability for the redox reaction of PA and 4-AP simultaneously.

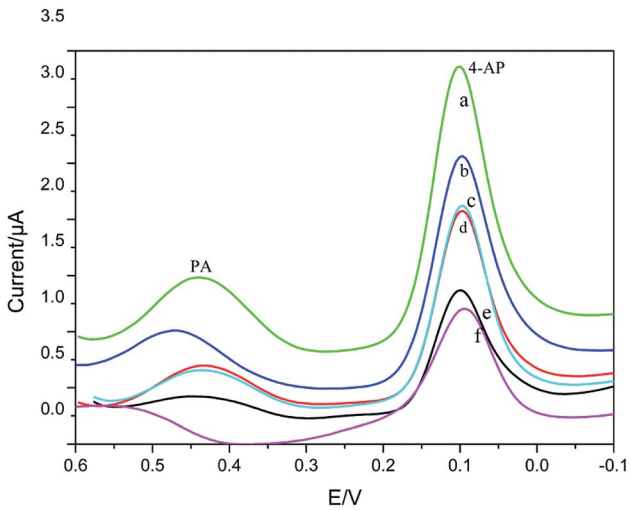

Fig. 5 DPVs of PA and 4-AP in PBS solution (pH = 8.0) containing 50 μM PA and 4-AP at CS/Ag–Pd@rGO/GCE (a), CS/Pd/rGO/GCE (b), CS/rGO/GCE (c), CS/Ag/rGO/GCE (d), CS/GCE (e) and GCE (f), respectively.

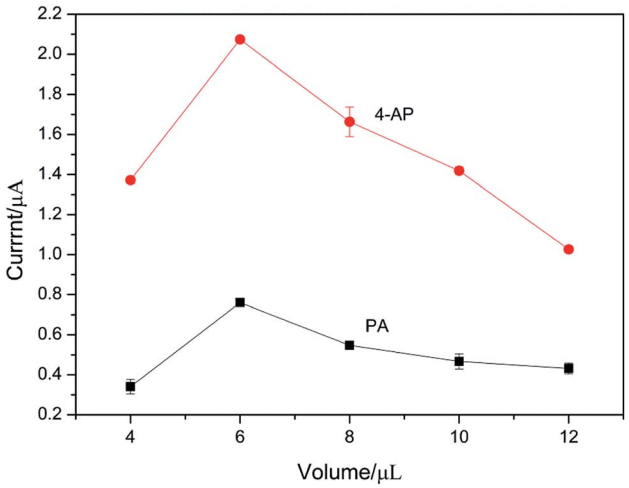

Fig. 6 Effect of dosage of Ag–Pd@rGO/GCE.

3.3 Effect of dosage of Ag–Pd@rGO

The effect of the dosage of Ag–Pd@rGO on the oxidation peak current of PA and 4-AP was investigated experimentally. The modified electrodes were prepared with 4, 6, 8, 10, and 12 μL composite materials, respectively, and the electrochemical behaviors of PA and 4-AP were studied under the same conditions. The results are shown in Fig. 6. It can be seen clearly that the oxidation peak current increases with the dosage of Ag–

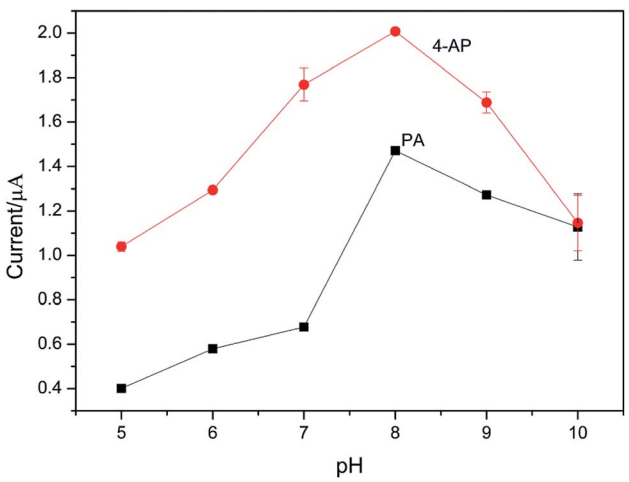

Fig. 7 The effect of pH on the peak current of mixture of 50 μM PA and 4-AP in PBS at CS/Ag–Pd@rGO/GCE.

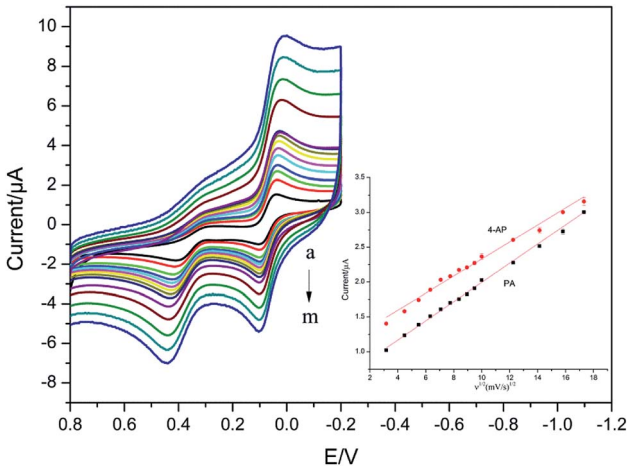

Fig. 8 CVs of CS/Ag–Pd@rGO/GCE in the PBS containing PA and 4-AP at different scan rates. Inset was the plot of anodic peak current density *vs.* square root of scan rates for PA and 4-AP.

Pd@rGO and gradually decreases after reaching the maximum value. This is because that the increase of the electrode material can increase the catalytically active sites for the redox of PA and 4-AP. However, when the Ag–Pd@rGO film is too thick, the electron transport rate is impeded, resulting in a decrease of response current. Therefore, 6 μL was selected as the optimum amount of modification.

3.4 Effect of pH value

The effect of pH on the electrochemical response at CS/Ag–Pd@rGO/GCE in 50 μM PA and 50 μM 4-AP in PBS was investigated experimentally, with a pH range of 5.0 to 10.0. It can be seen from Fig. 7 that the oxidation peak current increases with increasing pH and reaches a maximum at pH 8.0. When the pH continues to increase, all the oxidation peak currents of PA and 4-AP decrease. That is because that PA and 4-AP are weak acids that can ionize protons. When the pH of the PBS substrate is lower, the ionization equilibrium of PA and 4-AP shifts to the left; when the pH is larger, excessive OH^- hinders the reaction. Therefore, pH significantly affects the catalytic process of Ag–Pd@rGO. Considering the sensitivity of the electrode, a pH of 8.0 is selected as the optimum electrolyte solution.

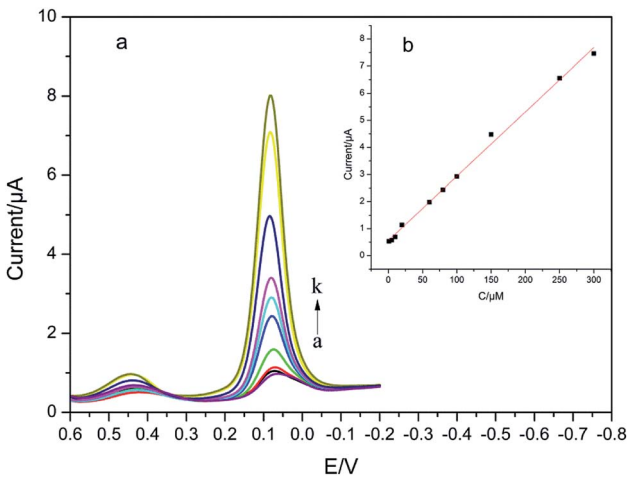

Fig. 9 DPVs for modified with CS/Ag–Pd@rGO/GCE in 0.1 M PBS (pH = 8.0) containing different concentrations of 4-AP (1.00 → 300.00 μM) and 50 μM PA, and its corresponding calibrating plot.

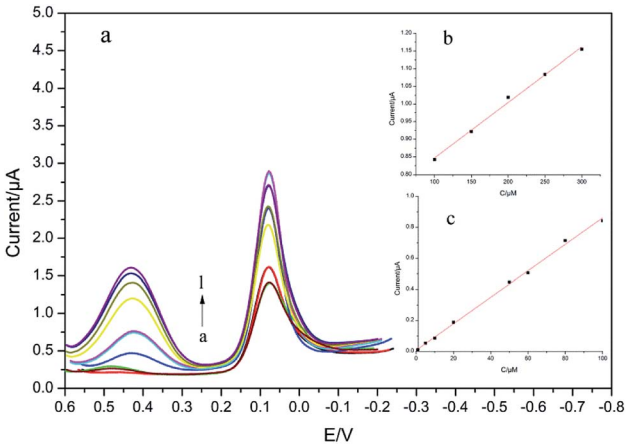

Fig. 10 DPVs for modified with CS/Ag–Pd@rGO/GCE in 0.1 M PBS (pH = 8.0) containing different concentrations of PA (0.50 → 300.00 μM) and 50 μM 4-AP, and its corresponding calibrating plot.

Table 1 Simultaneous detection of PA and 4-AP with the standard addition method

PA			4-AP		
Added (μM)	Found (μM)	Recovery (%)	Added (μM)	Found (μM)	Recovery (%)
20.0	19.8	99.0	20.0	20.4	102.0
60.0	59.7	99.5	60.0	58.7	97.8
100.0	99.7	99.7	100.0	100.4	100.4

3.5 Influence of scan rate

The effect of scan rate on the redox reaction of 4-AP and PA was researched at CS/Ag–Pd@rGO/GCE by CV. It can be seen from Fig. 8 that both the oxidation peak currents of PA and 4-AP increase with the increase of scanning rate. When the scanning rate is 10–300 mV s^{-1}, the oxidation peak current of PA and 4-AP

Table 2 Detection of PA in paracetamol tablet samples

Sample	Added (mg per tablet)	Found (mg per tablet)	R. S. D. (%)
Paracetamol	500.0	500.0	6.56
		498.9	
		533.7	
		464.4	
		451.8	
		541.3	

Table 3 Compared with different electrochemical analysis methods for the detection of PA or/and 4-AP

Modified electrodes	Analyte	Linear range (μM)	Detection limit (μM)	Reference
MCPE/PR	PA	0.7–100	0.53	30
NCOS/GCE	PA	0.5–600	0.157	31
EFTACPE	PA	1–150	0.5	32
POROUS GOLD NANOSHEETS/GCE	PA	3–320	0.23	33
CSs@ MoS_2/GCE	4-AP	0.01–18	0.003	34
MoS_2@NHCSs/GCE	4-AP	0.05–20	0.020	35
	PA	0.05–20	0.013	
G-PANI/CPE	4-AP	50–500	15.68	36
CS/Au/Pd/rGO/GCE	4-AP	1–300	0.12	37
	PA	1–250	0.30	
CS/Ag–Pd@rGO/GCE	4-AP	1.00–300.00	0.013	This work
	PA	0.50–300.00	0.23	

is linear with the square root of the scanning rate with the linear equation of I_{pa} (μA) = 0.1377 $\nu^{1/2}$ (mV s^{-1})$^{1/2}$ + 0.6184 (R = 0.9991) and I_{pa} (μA) = 0.1222 $\nu^{1/2}$ (mV s^{-1})$^{1/2}$ + 1.1080 (R = 0.9919), respectively, which indicates that the electrode reactions of PA and 4-AP are controlled by diffusion.

3.6 Linear range and limit of detection

DPV generally has a higher detection sensitivity and better resolution than CV. Fig. 9a shows that the DPV curves of 4-AP with various concentrations, and the coexisted PA (50 μM) had no effect on the detection of 4-AP. As shown in Fig. 9b, the increase of I_{pa} fits the linear equation of I_{pa} (μA) = 0.024 × c (μM) + 0.5710 (R = 0.9957) when the concentrations of 4-AP were in the range of 1.00–300.00 μM with the detection limit of 0.013 μM (S/N = 3) was obtained.

Analogously, Fig. 10a shows DPV responses for different concentrations of PA under the existence of 50 μM 4-AP. The linear range of PA was from 0.5 to 300 μM with a regression equation of I_{pa} (μA) = 0.009 × c (μM) + 0.0075 (R = 0.9980, 0.5–100.00 μM, Fig. 10b) and I_{pa} (μA) = 0.002 × c (μM) + 0.6894 (R = 0.9937, 100.00–300.00 μM, Fig. 10c) and a detection limit of 0.23 μM (S/N = 3).

3.7 Recovery test and real samples analysis

In order to assess the recovery of this method, the CS/Ag–Pd@rGO/GCE was used to detection 4-AP (50 μM) and PA (50 μM) in water samples. On a account of no response for 4-AP and PA were observed in water samples,[37] using the standard addition method for testing recovery and the results were listed in Table 1. The recovery tests of 4-AP and PA were between 97.8%–102.0% and 99.0%–99.7%, respectively. The results show that the method has higher accuracy.

DPV method was used to measure the amount of PA in the pharmaceutical preparation to verify the analytical performance of the modified electrode. The content of PA in a paracetamol tablet was detected according to the previous method of our research group.[37] The results are shown in Table 2. The measurement results were basically consistent with the paracetamol content specified by the manufacturer, and the relative standard deviation (RSD) of the six parallel test samples was less than 6.56%.

3.8 Reproducibility, stability and interference effect

In order to appraise the reproducibility of the modified electrode, a CS/Ag–Pd@rGO/GCE was measured 6 times in PBS samples containing 50 μM PA and 4-AP (pH 8.0), and the RSDs of PA and 4-AP were 0.87% and 0.33%, respectively.

To measure the stability of the electrode, CS/Ag–Pd@rGO/GCE was placed under the condition of 4 °C for 20 days, and the oxidation peak current values of PA and 4-ap measured by DPV method were 94.8% and 96.3% of the initial value respectively.

In order to evaluate the interference effect of the electrode, the influence of some interfering substances on the experiment was tested. It was found that 1000-fold concentrations of NaCl, KCl, $Cu(SO_4)_2$, $CaCl_2$, urea, glucose, ascorbic acid, 100-fold concentration of tyrosine and L-cysteine did not affect the determination of PA and 4-AP (signal change below 5.0%).100-fold concentration of catechol did not affect the determination of PA and 4-AP (signal change below 7.8%).

The above experimental results show that CS/Ag–Pd@rGO/GCE has good reproducibility, stability and interference effect.

3.9 Compared with other methods

This method has a wider linear range and a lower detection limit than other electrochemical analysis methods for detecting PA and 4-AP,[30–37] as showed in Table 3.

4. Conclusions

In this work, a sensitive and reliable electrochemical sensor was designed to detect the electrochemical redox of PA and 4-AP at CS/Ag–Pd@rGO/GCE. For simultaneous determination of PA and 4-AP, CS/Ag–Pd@rGO/GCE showed better electrochemical performance compared to the other modified and bare GCE. Under optimized conditions, CS/Ag–Pd@rGO/GCE exhibited wide linear range and low detection. In addition, CS/Ag–Pd@rGO/GCE showed high stability, high reproducibility and high anti-interference ability. All the results indicate that CS/

Ag–Pd@rGO/GCE has potential application value in electrochemical sensor field.

Conflicts of interest

The author(s) declare that they have no competing interests.

Acknowledgements

This work was supported by College Science and technology innovation team program of Henan Province (No. 14IRTSTHN030).

References

1 L. Y. Shiroma, M. Santhiago, A. L. Gobbi and L. T. Kubota, *Anal. Chim. Acta*, 2012, **725**, 44–50.
2 A. U. Alam, Y. Qin, M. M. R. Howlader, N. X. Hu and M. J. Deen, *Sens. Actuators, B*, 2018, **254**, 896–909.
3 P. Rattanarat, A. Suea-Ngam, N. Ruecha, N. Ruecha, W. Siangproh, C. S. Henry, M. Srisa-Art and O. Chailapakul, *Anal. Chim. Acta*, 2016, **925**, 51–60.
4 M. Siepsiak, E. Szałek, A. Karbownik, T. Grabowski, M. Mziray, K. Adrych and E. Grześkowiak, *Pharmacol. Rep.*, 2016, **68**, 733–736.
5 S. Prabakar and S. Narayanan, *Talanta*, 2007, **72**, 1818–1827.
6 T. Németh, P. Jankovics and J. Németh-Palotás, *J. Pharm. Biomed. Anal.*, 2008, **47**, 746–749.
7 Y. Fan, J.-H. Liu, C.-P. Yang, M. Yu and P. Liu, *Sens. Actuators, B*, 2011, **157**, 669–674.
8 M. Pasandideh-Nadamani, A. Omrani and M. R. Sadeghi-Maleki, *Anal. Biochem.*, 2016, **502**, 36–42.
9 P. Shaikshavali, T. M. Reddy, V. N. Palakollu, R. Karpoormath, Y. S. Rao, G. Venkataprasad, T. V. Gopal and P. Gopal, *Synth. Met.*, 2019, **252**, 29–39.
10 M. Zhou, Y. Zhai and S. Dong, *Anal. Chem.*, 2009, **81**, 5603–5613.
11 J. W. Suk, W. H. Lee and J. Lee, *Nano Lett.*, 2013, **13**, 1462–1467.
12 Q. Hong, L. Yang, L. Ge, Z. Liu and F. Li, *Analyst*, 2018, **143**, 3327–3334.
13 H. Lv, X. Zhang, Y. Li, Y. Ren, C. Zhang, P. Wang, Z. Xu, X. Li, Z. Chen and Y. Dong, *Microchim. Acta*, 2019, **186**, 416.
14 H. A. Becerril, J. Mao and Z. Liu, *ACS Nano*, 2008, **2**, 463–470.
15 X. C. Zhou, X. L. Yan, Z. S. Hong, X. Y. Zheng and F. Wang, *Sens. Actuators, B*, 2018, **255**, 2959–2962.
16 M. Dharshini, T. Nurulkhalilah and S. Yusran, *Synth. Met.*, 2019, **252**, 76–81.
17 H. J. Wang, S. Y. Zhang, S. F. Li and J. Y. Qu, *Anal. Methods*, 2018, **10**, 1331–1338.
18 Y. Wang, J. H. Qu, S. F. Li, Y. Dong and J. Y. Qu, *Microchim. Acta*, 2015, **182**, 2277–2283.
19 Y. H. Yi, D. P. Zhang, Y. Z. Ma, X. Y. Wu and G. B. Zhu, *Anal. Chem.*, 2019, **91**, 2908–2915.
20 X. Chen, G. Wu, J. Chen, X. Chen, Z. Xie and X. Wang, *J. Am. Chem. Soc.*, 2011, **133**, 3693–3695.
21 N. Miyaura and A. Suzuki, *Chem. Rev.*, 1995, **95**, 2457–2483.
22 M. X. Chen, Z. Zhang, L. Z. Li, Y. Liu, W. Wang and J. P. Gao, *RSC Adv.*, 2014, **4**, 30914–30922.
23 N. T. S. Phan, M. V. D. Sluys and C. W. Jones, *Adv. Synth. Catal.*, 2006, **348**, 609–679.
24 H. Y. Wang, D. L. Chen, Y. J. Wei, L. Q. Yu, P. Zhang and J. L. Zhao, *Spectrochim. Acta, Part A*, 2011, **79**, 2012–2016.
25 H. Choi, T. Kang, K. Um, J. Kim and K. Lee, *Colloids Surf., A*, 2014, **459**, 120–127.
26 G. O. Martins, M. S. Petrônio, A. M. F. Lima, A. M. M. Junior, V. A. O. Tiera, M. F. Calmon, P. S. L. Vilamaior, S. W. Hanc and M. J. Tiera, *Carbohydr. Polym.*, 2019, **216**, 332–342.
27 S. W. Yu, X. L. Xu, J. F. Feng, M. Liu and K. L. Hu, *Int. J. Pharm.*, 2019, **560**, 282–293.
28 G. Ma, C. D. Qiao, X. J. Wang, J. S. Yao and J. Xu, *Int. J. Biol. Macromol.*, 2019, **135**, 240–245.
29 S. Pei and H. Cheng, *Carbon*, 2012, **50**, 3210–3228.
30 T. Thomas, R. J. Mascarenhas, F. Cotta, K. S. Guha, B. E. K. Swamy, P. Martis and Z. Mekhalif, *Colloids Surf., B*, 2013, **101**, 91–96.
31 L. Fu, A. Wang, G. Lai, C. Lin, J. Yu, A. Yu, Z. Liu, K. Xie and W. Su, *Microchim. Acta*, 2018, **185**, 87.
32 K. Movlaee, H. Beitollahi, M. R. Ganjali and P. Norouzi, *Microchim. Acta*, 2017, **184**, 3281–3289.
33 Q. Zhang, J. Feng, A. Wang, J. Wei, Z. Lv and J. Feng, *Microchim. Acta*, 2015, **182**, 589–595.
34 J. J. Qian, D. P. Zhang, L. R. Liu, Y. H. Yi, M. N. Fiston, O. J. Kingsford and G. B. Zhu, *J. Electrochem. Soc.*, 2018, **165**(11), B491–B497.
35 D. P. Zhang, J. J. Qian, Y. H. Yi, O. J. Kingsford and G. B. Zhu, *J. Electroanal. Chem.*, 2019, **847**, 113229.
36 M. Nemakal, S. Aralekallu, I. Mohammed, M. Pari, K. R. Reddy and L. K. Sannegowda, *Electrochim. Acta*, 2019, **318**, 342–353.
37 H. J. Wang, S. Y. Zhang, S. F. Li and J. Y. Qu, *Talanta*, 2018, **178**, 188–194.

